

WYLE LABORATORIES - RESEARCH STAFF
Report WR 66-35


THE FLUCTUATING PRESSURES
DUE TO SHOCK INTERACTIONS
WITH TURBULENCE AND SOUND

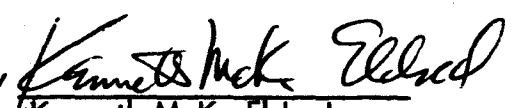
By

M. V. Lawson

Work Performed Under Contract NAS8-11308

Prepared by M. V. Lawson
M. V. Lawson

Approved by 
L. C. Sutherland
Research Operations Manager

Approved by 
Kenneth McK. Eldred
Director of Research

June, 1966

COPY NO. 4

SUMMARY

34641

High levels of pressure fluctuation have been observed on surfaces beneath shock waves in turbulent flow. These levels contribute substantially to the buffet loadings experienced by aircraft and space vehicles in transonic and supersonic flight. It has usually been suggested that these fluctuations are associated with an oscillating shock phenomenon. However, it is shown here that the interaction between the turbulence and shock is sufficient to account for the observed fluctuating pressure field. Computations have been performed following the methods of Ribner (NACA Rept. No. 1233), but explicitly including the nearfield pressure terms. It has been found that, for instance, the interaction of turbulence of intensity 0.05 with a typical separation shock at $M = 2.0$ will generate a near field noise level of 164 dB. The contribution of shock motion, due to turbulence, to surface pressure fluctuations has been studied. The interaction between shocks and sound has been studied following Moore (NACA Rept. No. 1165). The predicted magnification of incident sound behind the shock (4.5 dB for a $M = 2.0$ separation shock) is probably sufficient to account for the observed "sensitivity of an oscillating shock to wind-tunnel noise".

TABLE OF CONTENTS

	Page Number
SUMMARY	ii
TABLE OF CONTENTS	iii
LIST OF FIGURES	iv
1.0 INTRODUCTION	1
2.0 SHOCK-TURBULENCE INTERACTION	2
2.1 Ribner's Theory for Shock Turbulence Interaction	2
2.2 Practical Consequences	4
2.3 Effect of Shock Movement	6
3.0 THE INTERACTION OF SOUND WAVES AND A SHOCK	10
4.0 CONCLUSIONS	12
REFERENCES	14

LIST OF FIGURES

	Page Number
Figure 1 Interaction of a Shear Wave with a Shock	16
Figure 2 Wave Angles at Critical Condition, Shock-Shear Wave Interaction	17
Figure 3 Refracted versus Initial Shear Wave Angle, Shock Shear Wave Interaction	18
Figure 4 Sound Wave Angle versus Initial Shear Wave Angle Shock-Shear Wave Interaction	19
Figure 5 Amplitude of Shock Motion versus Initial Shear Wave Angle, Shock-Shear Wave Interaction	20
Figure 6 Pressure Fluctuation versus Shear Wave Angle, Shock-Shear Wave Interaction	21
Figure 7 Near and Far Field Sound Level for Shock Interaction With Unit Isotropic Turbulence	22
Figure 8 Separation Shock Angle versus Mach Number	23
Figure 9 Turbulence Intensities in Separating and Attached Subsonic Boundary Layers	24
Figure 10 Calculated Near-Field Sound Levels at a Typical Separation Shock	25
Figure 11 Comparison of Experimental Results with Present Theory at Supersonic Speeds	26
Figure 12 Fluctuating Pressure Under Transonic Oscillating Shock versus Mach Number	27
Figure 13 Amplitude versus Mach Number for Shock Turbulence Interaction	28
Figure 14 Interaction of a Sound Wave With a Shock	29

LIST OF FIGURES (Continued)

		Page Number
Figure 15	Critical Conditions for Shock-Sound Interactions	30
Figure 16	Incident and Refracted Wave Angles for Shock Sound Interaction	31
Figure 17	Pressure Magnification Factor versus Incident Sound Wave Angle, Shock-Sound Interaction	32
Figure 18	Range of Magnification Factor for Shock Sound Interaction	33

1.0 INTRODUCTION

Both external and internal supersonic flows will, typically, contain shock waves and these shock waves are frequently under some form of disturbance. In many cases of practical importance the shock may interact with a turbulent boundary layer at a surface. Free stream turbulence may also be present and, particularly in internal flows, sound waves may propagate in the free flow. A shock disturbance problem of particular interest to the present study is that of a large launch vehicle moving at supersonic velocities. Here, the separation shocks forming in front of the inter-stage flares interact with both the separating turbulent boundary layer, and with the turbulent wakes shed from upstream protuberances notably the escape tower.

Prediction of the characteristics of such shock interactions is clearly of practical interest. Fortunately, the foundation for such a study has been laid in work by Ribner (References 1 and 2) and Moore (Reference 3). In Reference 1, Ribner studied the interaction of a shear wave with a shock, and demonstrated the existence of both sound waves, and refracted "shear-entropy" waves in the flow behind the shock. In Reference 2, Ribner generalized this work to give the noise radiated by the interaction of a shock with turbulence. Moore (Reference 3) studied the interaction of sound with a shock wave. His results showed the same broad features as those of Ribner for the turbulence interaction.

The major interest of the present investigation is in the pressure fields generated by the interaction effects. The fluctuating surface pressure field associated with a shock is thought to be the cause of several catastrophic failures of launch vehicles accelerating through the "max q" region. It seems possible that a large proportion of the experimentally observed fluctuating pressure field could be due to shock turbulence interaction.

Although the theoretical work necessary for this study has already been substantially accomplished by Ribner and Moore, relatively little numerical information was given in their reports. In particular, Ribner calculated only the far-field sound pressure due to shock turbulence interaction (Reference 2). The surface pressure field near the shock would be related to the near-field pressures due to the interaction, and these are calculated in the present report. In addition, the motion of the shock during the interaction has been analyzed. For reasons to be discussed below, only the far-field is of interest in the shock sound interaction. Moore gives both near and far-field characteristics in his report (Reference 3), but his numerical calculations were essentially limited to Mach numbers of 1, 1.5, and ∞ , so that the need for further numerical calculations is apparent.

Thus, this report presents extended numerical results for the interaction of both turbulence and sound with a shock. It will be shown that the fluctuating pressure field from both interaction effects is of practical significance in typical supersonic flow problems.

2.0 SHOCK-TURBULENCE INTERACTION

2.1 Ribner's Theory for Shock Turbulence Interaction

Ribner's theories are fully described in References 1 and 2. The broad features underlying the theory are repeated here to assist later interpretation. Disturbances in a supersonic flow may be divided into types, as demonstrated by Kovasznay (Reference 4). The three fundamental modes are vorticity, entropy, and sound. The shock equations couple these modes together so that input of any one mode of disturbance into the shock will generally give rise to all three modes of disturbance behind the shock. Turbulence may be characterized as the vorticity disturbance mode, and it is of interest, first of all, to consider an elementary disturbance of this type, the shear wave. Figure 1 shows a single shear wave being swept into a shock by the free stream. If the shear wave lies at an inclination θ to the shock, then it can be seen that the shock front will experience a wave moving along its length.

As discussed above, the simple shear wave entering the shock will give rise to vorticity, entropy, and sound disturbances behind the shock. Immediately behind the shock, these disturbances must combine to be in phase with the input shear wave. Now if the phase velocity of the wave motion along the shock is sufficiently high, then the individual sound disturbances behind the shock can combine to give radiated plane sound waves, as shown in Figure 1. Alternatively, if this phase velocity is less than some critical value, then no coupling into radiated sound waves is possible and, instead, an exponentially decaying "pressure wave" field will be generated. These two types of sound radiation may be regarded as the far and near-field components, respectively.

The input shear wave also gives rise to a refracted "shear-entropy" wave which carries away the "frozen" patterns of vorticity and entropy generated immediately behind the shock. The refraction occurs because of the differential effect of the shock on the velocity components normal and parallel to it. Note that, at this stage, we consider only normal shocks. The oblique case may be obtained simply by superimposing a uniform velocity parallel to the shock front.

It is clear, therefore, that the form of the sound field behind the shock depends directly on the angle at which the shear wave enters the shock. The critical angle is given as a function of Mach number in Figure 2. Shear waves entering the shock at angles less than the critical angle will give decaying near-field pressure waves, while entry at greater angles will give rise to radiated acoustic waves. Figure 2 also shows the angles of the refracted shear-entropy wave and the sound wave at the critical condition.

Ribner's solution for the single shear wave involves considerable algebra, and will not be repeated here. Basically, he solves the linearized equations for compressible flow, including vorticity, downstream of the shock under boundary conditions imposed by the shear wave. These conditions immediately behind the shock are found by a linearized version of the normal shock wave relations. Complete details may be found in Reference 1, and the present work has involved computation, using Ribner's equations.* Some of Ribner's equations have been rewritten in a more convenient form using the well known oblique shock wave relations (e.g. Reference 5).

Computed results from this theory are presented in Figures 3 through 6, giving the shear wave and sound wave angles, the non-dimensional vibration amplitude and the pressure contribution immediately behind the shock. In each of these, it can be seen that the incident angle of the sound wave has a crucial effect on the observed properties, and that, in general, disturbances immediately behind the shock are greater when the incident angle is low. This regime corresponds to the subcritical case with a decaying pressure wave generated behind the shock.

In Figure 4, the sound wave angle has also been plotted for subcritical shear wave angles. In this case, the angle corresponds to lines of constant phase, along which the sound decays exponentially. The non-dimensionalized amplitude plotted in Figure 5 is $(a^2 + b^2)^{0.5}$ in Ribner's notation (Reference 1). It must be multiplied by the r.m.s. value of turbulence intensity and divided by the wave number of the shear wave under consideration to give the actual shock vibration amplitude. The pressure perturbation given in Figure 6 has been non-dimensionalized by division by the static pressure behind the shock, and also requires multiplication by the r.m.s. turbulence intensity to give the actual pressure perturbation in any case. The peculiar peaks occurring in the amplitude and pressure graphs near the critical condition, at high Mach numbers, have been studied in detail and have found to be a real theoretical effect and not a result of the computational procedure.

*Note that Reference 1 contains a misprint, in equation 35. The $(m - 1)$ term in the expression for E' should be squared. This misprint does not affect the calculations either in Ribner's or the present work.

In Reference 2, Ribner generalized his results for the single shear wave to cover the case of random turbulent motion. Turbulence may be regarded as a random assemblage of shear waves at all angles of incidence as discussed, for example, in Reference 6. The theoretical development for this case was a direct statistical generalization of the work in Reference 1, and Ribner gives formulae for the random velocity, temperature, and far sound pressure fields behind the shock for the cases of both isotropic and strongly asymmetric turbulence. For the latter case, Ribner calculated results corresponding to lateral components being 36.1 times stronger than the longitudinal components, but found little difference between that and the isotropic case with the same longitudinal intensity. This result may be understood by Reference to Figures 5 and 6. Clearly, the shear waves components entering at low angles have the maximum effect. Thus, the longitudinal components of the turbulence would likewise be expected to have the maximum effect, as observed.

Figure 7, computed using Ribner's formulae, gives the far-field sound for shock turbulence interaction as a function of the upstream normal Mach number. The sound pressure is given as p_{rms}/q , the root mean square pressure divided by the total head of the upstream flow component normal to the shock, and corresponds to unit turbulence intensity. Here the usual definition of turbulence intensity as root mean square velocity fluctuation divided by the upstream flow velocity (here normal to the shock) has been used. For the present purposes, an estimate of the near-field pressure is required, and this can be computed, using formulae in Ribner's paper. The fluctuating pressure field immediately behind the shock is also given as a function of Mach number in Figure 7. It may be immediately observed that this near-field level is significantly higher than the far-field level, and the practical consequences of this observation are the main object of interest in the present report.

2.2 Practical Consequences

The majority of real flows contain shocks at oblique angles to the free stream direction. Thus, the results above cannot be applied directly. Since velocities parallel to the shock front have no effect on the calculations, all that is required is the definition of the velocities normal to the shock for each case and appropriate allowance in both the pressure generation and turbulence intensity. A typical practical problem is the interaction of a supersonic separating turbulent boundary layer with its associated separation shock. Results for the observed shock angle for this case are available in References 7 and 8 and are shown in Figure 8, together with an empirical curve. The actual turbulence intensity is not known for the supersonic case, but some subsonic results (References 9 and 10) are shown in Figure 9. Perhaps the most suitable assumption would be that the intensity is equal to that of the subsonic separating boundary layer shown in Figure 9, so that an intensity of 0.05 would be very reasonable. Using the separation angles given in Figure 8, typical actual sound pressure levels are shown in Figure 10 as a function of Mach number for various turbulence intensities. The value of total head has been taken as 37,500 N/m² (800 psf) and is typical of a large launch vehicle in the low supersonic Mach number range. It will be observed that a level of 164 dB occurs immediately behind the

shock for $M = 2.0$, assuming a turbulence intensity of 0.05. For a real space vehicle, the intensity of the turbulence impinging onto the shock could be very much higher, due to the turbulent wake from upstream protuberances, notably the escape tower. A value of turbulence intensity of at least 0.1 would not be unreasonable.

However, at this stage, it should be noted that the near-field values given here are not necessarily equal to the pressure fluctuation observed at the vehicle surface. The near pressure field decays exponentially as it passes downstream from the shock and, more importantly, the shock only penetrates part way into the boundary layer. Ribner's theory, in its present form, does not apply to this case, and any extension of the theory seems unlikely to give significantly improved results, particularly in view of the lack of any relevant experimental data for the parameters involved. Consequently, no numerical results for these real shock effects are presently available. However, it does appear that the pressure fluctuation levels for low frequencies, with wave lengths greater than the local boundary layer thickness, will be substantially equal to the levels given here. Since these frequencies are usually of predominant importance in structural response, the limitation discussed above may be of minor practical consequence. In addition, the shock waves in front of small angle flares ($< 20^\circ$ say) lie close to the whole flare surface. Thus, pressure fluctuations due to shock turbulence interactions may cause significant loading along the whole length of the flare. This supposition is borne out by the appearance of the flow field for these cases under shadowgraph visualization, where an extensive region of density perturbation can be seen to lie along the flare (Reference 7).

An objection to the practical utility of these theories is provided by experimental results on peak surface pressure fluctuations under separation shocks. Figure 11 shows typical unpublished results obtained by C. Coe at NASA Ames Research Center, together with the present theoretical results assuming a constant value of turbulence intensity at 0.04. The experimental results were obtained with a smooth body before the flare, and it is not unreasonable to suppose that the turbulence level would be near that assumed. However, the experimentally observed reduction in level with reduction in Mach number is not shown in the theory. A possible explanation for this may be found in Figure 4. Here it may be seen that the sound behind the shock is scattered over a wider angular range at low Mach numbers. In addition, it might be supposed that the shock would penetrate less far into the boundary layer at the low Mach numbers, and thus encounter less severe turbulence intensities. Both these effects would tend to reduce the peak fluctuation level observed.

However, results presented by Jones and Foughner (Reference 11) for transonic fluctuation on the Saturn vehicle can be conveniently explained, in principle, by the present work. It was found that the presence of the wake from the escape tower could not be detected in surface pressure fluctuation measurements taken beneath "smooth" flow several diameters back from the nose. But its presence could be detected in the pressure fluctuations beneath the shocks behind the second shoulder. The explanation of this effect in terms of a shock-turbulence interaction phenomenon is apparent.

It is of interest to apply the present results to the surface pressure fluctuations beneath a transonic "oscillating shock". Figure 12 gives an estimate of the fluctuating pressure level against Mach number. Here it has been assumed that the transonic shock terminating a locally supersonic region is such that it is normal, and the velocity behind it is equal to the free stream Mach number. The curve assumes a constant turbulence intensity of 0.01, referred to the free stream velocity. Also shown are a number of experimental results from References 12 to 14. Note that these results refer to the peak fluctuating pressure immediately beneath the shock and do not include the case of alternating flow separation and attachment (Reference 15) which is not thought to be of practical importance (References 11 and 16). Reference 16 gives a more complete discussion of the data.

Figure 12 cannot be said to show more than a very broad agreement with the present theories. However, it is of interest that turbulence intensities as low as 0.01 can generate such large levels of near-field fluctuating pressure. The observed scatter in the experimental results might also be explained in terms of the varying turbulence intensity in the experiments, as discussed above for the case of the wake from the escape tower.

2.3 Effect of Shock Movement

Although the leading features of the near-field pressure fluctuation have been described, the results presented here have been subject to considerable interpretation and restrictions in any practical case. One additional effect, not considered so far, is the effect of shock motion. This is of interest on two counts. First, actual shock motion near the surface will lead to the imposition of fluctuating pressures at the surface due to the switching from the high to the low pressure side of the shock wave. This general mechanism has been discussed by Kistler (Reference 17), although the practical application of his results seems doubtful (Reference 16). Second, the motion of the shock can be recorded during experiment, thus enabling a direct comparison with theory.

In Reference 1, Ribner gives formulae for the motion of the shock front. However, these were not generalized for the random case, and the necessary development is laid out below.

This analysis broadly follows the analysis of Ribner (Reference 2) with some changes in notation. Batchelor (Reference 6) gives the spectral density tensor of isotropic turbulence as

$$\Phi_{ij}(k) = \frac{E(k)}{4\pi k^4} (k^2 \delta_{ij} - k_i k_j) \quad (1)$$

Where $E(k)$ is the energy spectrum level and k a wave number.

Thus, if the vector wave number is $\underline{k} = -k \sin \theta, k \cos \theta \cos \phi, k \cos \theta \sin \phi$ (2) then the longitudinal spectral density may be written

$$\Phi_{11}(k) = \frac{E(k)}{k^2} \cos^2 \theta \quad (3)$$

The mean square longitudinal velocity (non-dimensional) may be written

$$\overline{u^2} = \int \Phi_{11}(k) d\underline{k} \quad (4)$$

Also Ribner shows, in Equation (41) of Reference 1, that in the present notation, the amplitude of the shock motion is

$$x = u \frac{\sqrt{a^2 + b^2}}{k \cos \theta} \quad (5)$$

where a and b are shock perturbation parameters as defined in Reference 1.

$$\text{Thus } \overline{x^2} = \int \Phi_{11}(k) \frac{(a^2 + b^2)}{k^2 \cos^2 \theta} d\underline{k} \quad (6)$$

From (2) $d\underline{k} = k^2 \cos \theta dk d\phi d\theta$, and using this and (3) in Equation (4) and (6) gives

$$\overline{u^2} = \int_0^\infty E(k) dk \int_0^{2\pi} d\phi \int_0^\pi \cos^3 \theta d\theta \quad (7)$$

$$\text{and } \overline{x^2} = \int_0^\infty \frac{E(k)}{k^2} dk \int_0^{2\pi} d\phi \int_0^\pi (a^2 + b^2) \cos \theta d\theta$$

Thus defining a "mean wave number" by

$$\overline{k^2} = \frac{\int_0^\infty E(k) dk}{\int_0^\infty \frac{E(k)}{k^2} dk} \quad (8)$$

gives

$$\frac{\overline{k^2} \overline{x^2}}{\overline{u^2}} = \frac{3}{2} \int_0^{\pi/2} (a^2 + b^2) \cos \theta d\theta \quad (9)$$

where the limits of integration have been changed to 0 and $\pi/2$ and the integral doubled because of the symmetry in θ .

Equation 9 gives the desired formula for the non-dimensional amplitude of the random motion of a shock. A computed graph of this parameter is given in Figure 13 as a function of Mach number.

Unfortunately, the practical application of these results is not straightforward. Equation (8) defines a "mean wave number" which characterizes the spectrum of the upstream turbulence. Present experimental results, for instance Reference 18, give the energy spectrum $E(k)$ of the turbulence, so that evaluation of Equation (8) would appear simple. However, these results suggest that the energy/unit wave number is substantially constant over the low frequency range, down to the experimental low frequency limit (1 cps in Reference 18). Since the square of the wave number appears as a divisor in the bottom integral of Equation (8), it will be observed that the numerical value of the "mean wave number" is critically dependent on the exact form assumed for the energy spectrum between zero and the lower experimental limits. This value will be near the value of k for which the energy spectrum level is rising proportionally to k^2 . It is possible to make broad statements about the magnitude of the integral using the mean value theorems, but these do not seem to add any significant information. However, it is of interest to note that a restriction to non-singular amplitudes at zero wave number does require the energy spectrum level to approach the origin at a rate greater than k^2 . This result appears to be of general application in all turbulence problems. Maestrello found (in unpublished work) a dependency of the low frequency turbulent pressure fluctuations on both Reynolds number and Mach number and this observation indicates still further complications.

In the present case, it appears that the "mean wave number" will be small. Another conclusion is that the shock displacements will be particularly sensitive to low frequency turbulence, for example, the escape tower wake. The surface pressures induced by this shock motion will clearly be significant. In Reference 17, Kistler calculates the surface pressure due to sinusoidal motion of a step pressure pulse. In fact, because of boundary layer effects, it is unlikely that the instantaneous pressure rise across the shock in the free stream will appear as a step pressure rise on the surface. The pressure rise may be expected to occupy a finite length of surface in the steady case. For small amplitude shock motions the resultant fluctuating surface pressure will therefore be considerably lower in level than predicted by Kistler, while for shock motion amplitudes greater than the extent of the pressure rise, the peak pressure fluctuation will be approximately equal to that predicted by Kistler, reaching $p_{rms}/q = 0.1$ or greater under various reasonable assumptions, (see Reference 17). It should also be noted that most experimental results demonstrate a relatively low peak frequency for the pressure fluctuations associated with a shock.

The surface pressure fluctuation due to shock motion is an effect which is additive to the near-field pressure. However, there is a phase relation between the two sources of pressure (Reference 1). The near-field pressure wave varies from being 180° out of phase with the shear wave velocity for $\theta = 0$ to being in phase for $\theta > \theta_{cr}$. If a linear mean pressure gradient is assumed, then the surface pressure due to shock motion would be 180° out of phase for $\theta = 0$ and 90° in advance for $\theta > \theta_{cr}$. Since the major part of both the motion amplitude and the near-field pressure arise from contributions with θ close to zero (see Figures 4 and 5), then the two sources will be substantially in phase, enabling them to be superposed directly.

Thus, although numerical results cannot be directly applied for the surface pressure problem, the arguments above do show that shock turbulence interactions can be a significant source of fluctuating surface pressure, particularly if the spectrum of the turbulence contains significant low frequency components.

THE INTERACTION OF SOUND WAVES AND A SHOCK

It is of interest to derive numerical results for the interaction of a shock with sound. The primary interest here is in the evaluation of fluctuating pressure results from wind tunnel tests in which wind tunnel noise may be present. The results are also of some general interest to supersonic internal flow systems.

A theoretical analysis of the sound shock interaction was developed by Moore in Reference 3, following independently the same broad lines as Ribner in Reference 1. Again the progression of the sound wave into the shock causes ripples to travel along the shock which can generate a decaying or radiating pressure field dependent on the angle of entry of the shock wave. Because the sound wave possesses a propagation velocity in addition to the convection velocity the values for the critical angle differ from the shock turbulence case. A further result of the propagation velocity is that it is possible for a sound wave to enter the shock from either upstream or downstream. Both cases are considered by Moore in Reference 3, but in the present work only the practically significant case, of sound passing into the shock from the upstream side, will be considered. Moore's results are generally limited to Mach numbers of 1, 1.5, and ∞ . More complete numerical calculations are therefore presented here, based on the formulae given by Moore in Reference 3.

Figure 15 gives the condition for radiated or decaying sound fields. It will be observed that the incident sound wave can be either large or small for radiated sound to occur. Virtually all practical cases involve sound traveling as plane waves in the free stream direction interacting with an oblique shock. Thus, the angle of incidence of the sound waves will be low. Therefore, only the results for radiated sound at lower angles of incidence are presented here. It should be noted that the mathematical model used here is close to the real case, and the results presented are therefore expected to be in close agreement with any experiment. Results immediately under the shock wave would be affected by shock motion as in the case of shock turbulence interaction above. Figure 16 gives the angle of the refracted sound wave. The change in angle of the sound wave will result in an increased phase velocity of sound over the surface, and this should be detectable by cross-correlation. However, the effect is relatively small, and probably of minor practical significance.

The key result of the present analysis is the predicted increase in sound pressure level that occurs behind the shock. The magnification factor is plotted against angle of incidence for various normal Mach numbers in Figure 17. The feature of this graph is substantial independence of the magnification factor on angle of incidence for low and moderate incidences. Using this observation, Figure 18 has been prepared to enable rapid estimation of the approximate magnification factor for any condition. Figure 18 is valid for angles of incidence between 0 and 80 degrees. Thus, for instance a typical $M = 2.0$ separation shock will have a normal Mach number of 1.35 (see Figure 8), and Figure 18 gives the magnification factor

for incident sound as about 4.5 dB.

A number of experimenters have observed increased levels of fluctuating surface pressure near shocks at frequencies associated with wind tunnel noise. This has been explained as a "sensitivity of an oscillating shock to wind tunnel noise". It appears that the predicted magnification factors due to shock sound interaction are sufficient to explain this effect without recourse to any oscillatory mechanisms within the shock. Unfortunately, no suitable experimental data are available to the writer to substantiate this point at present, but it is hoped that suitable experiments can be performed in the near future.

4.0 CONCLUSIONS

The near field fluctuating pressures due to the interaction of turbulence and sound with a shock wave have been calculated, following the theoretical work of Ribner and Moore (References 1, 2, and 3). The predicted pressure fluctuation levels for shock-turbulence interaction are high (164 dB for a $M = 2.0$ separation shock) and suggest that this mechanism could be responsible for the surface pressure fluctuations observed beneath shock waves.

The model used for the shock-turbulence interaction was quasi-one-dimensional and is not directly applicable to the fluctuations produced near the foot of a shock. Further, the actual shock motion will produce additional pressure fluctuations at the surface as the mean pressure gradient moves back and forth. Attempts to compute this second effect have demonstrated the particular significance of the low frequency turbulence, but no numerical results could be presented for this effect because of the lack of suitable experimental data.

The theory for the interactions should apply well to the cases where substantial lengths of a shock wave are effected by turbulence, for instance, the interaction of the separation shock with the wake from the escape tower on a launch vehicle. It may be noted that this theory predicts that major levels of fluctuating pressure will occur on the forward facing flares for this case. For all shock-turbulence interactions, theory predicts that the frequency spectrum of the fluctuating pressures, immediately behind the shock, will be equal to the turbulent velocity spectrum. Each near-field component decays exponentially so that the observed spectrum some distance from the shock will be dominated by the lower frequencies. Very far from the shock only radiated sound is present, and its spectrum is again equal to the input spectrum of the turbulence.

A study of the interaction of sound with a shock wave has shown that sound waves impinging on a shock are increased in intensity behind the shock. A $M = 2.0$ separation shock increases the sound intensity by about 4.5 dB. This effect offers a direct explanation of the observed "sensitivity of an oscillating shock to wind tunnel noise".

In general, the results of this study suggest that most of the observed fluctuation effects associated with shock waves can be explained directly in terms of various shock interactions. An effect of particular interest, not investigated here, is the possible interaction of a shock wave with local vehicle, or panel, motions. It appears that the shock could easily act as a "sounding board" for such motions and lead to some form of shock-panel instability, as suggested by analyses of some failures during flight.

The need for experimental data to support the theories presented here is apparent, and would have wide practical significance. Such experimental work is a logical next step in these investigations.

REFERENCES

1. Ribner, H. S.; "Convection of a Pattern of Vorticity Through a Shock Wave", NACA Rep. 1164, 1954.
2. Ribner, H. S.; "Shock-Turbulence Interaction and The Generation of Noise", NACA Rep. 1233, 1955.
3. Moore, F. K.; "Unsteady Oblique Interaction of a Shock Wave with a Plane Disturbance", NACA Rep. 1165, 1954.
4. Kovaszny, L.S.G.; "Turbulence in Supersonic Flow", J. Ae. Sci., Vol. 20, pp. 657-674, 1953.
5. Ames Research Staff: Equations, Tables and Charts for Compressible Flow, NACA Rep 1135, 1953.
6. Batchelor, G. K.; "The Theory of Homogeneous Turbulence", Cambridge University Press., 1960.
7. Kuehn, D. M.; "Turbulent Boundary Layer Separation Induced by Flares on Cylinders at Zero Angle of Attack", NASA TR-R117, 1961.
8. Lowson, M. V.; "Flow Visualization Experiments with Separated Supersonic Turbulent Flow", Wyle Research Report WR 66-23, April 1966.
9. Klebanoff, P. S.; "Characteristics of Turbulence in a Boundary Layer with Zero Pressure Gradient", NACA Rep. 1247, 1954.
10. Schubauer, G. B., and Klebanoff, P. S.; "Investigation of the Separation of a Turbulent Boundary Layer", NACA Rep. 1030, 1950
11. Jones, G. W. and Foughner, J. T.; "Investigation of Buffet Pressures on Models of Large Manned Launch Configurations", NASA TND-1633, May 1962.
12. Coe, C. F., and Kaskey, A. J.; "The Effects of Nose Bluntness on the Pressure Fluctuations Measured on 15° and 20° Cone-Cylinders at Transonic Speeds", NASA TMX-779, January 1963. (Declassified).
13. Coe, C. F., "Steady and Fluctuating Pressures at Transonic Speeds on Two Space Vehicle Payload Shapes", NASA TMX-503, 1961. (Declassified)

14. Coe, C. F., "The Effects of Some Variations in Launch Vehicle Mode Shape on Steady and Fluctuating Pressures at Transonic Speeds", NASA TMX-646, 1962. (Declassified).
15. Chevalier, H. L. and Robertson, J. E.; "Pressure Fluctuations Resulting From an Alternating Flow Separation and Attachment at Transonic Speeds", AEDC-TDR-63-204, November 1963.
16. Lowson, M. V., "The Acoustic Environment Due to Separated Flow and Oscillating Shocks", Wyle Research Report WR 66-8, March 1966.
17. Kistler, A. L., "Fluctuating Wall Pressure Under a Separated Supersonic Flow", J.A.S.A. Volume 36, pp. 543-550, March 1964.
18. Favre, A. J., Gaviglio, J. J., and Dumas, R.; "Space Time Double Correlations and Spectra in a Turbulent Boundary Layer", J. Fluid Mech., Volume 2, pp. 313-342, 1957, also J. Fluid Mech., Volume 3, pp. 344-356, 1958.

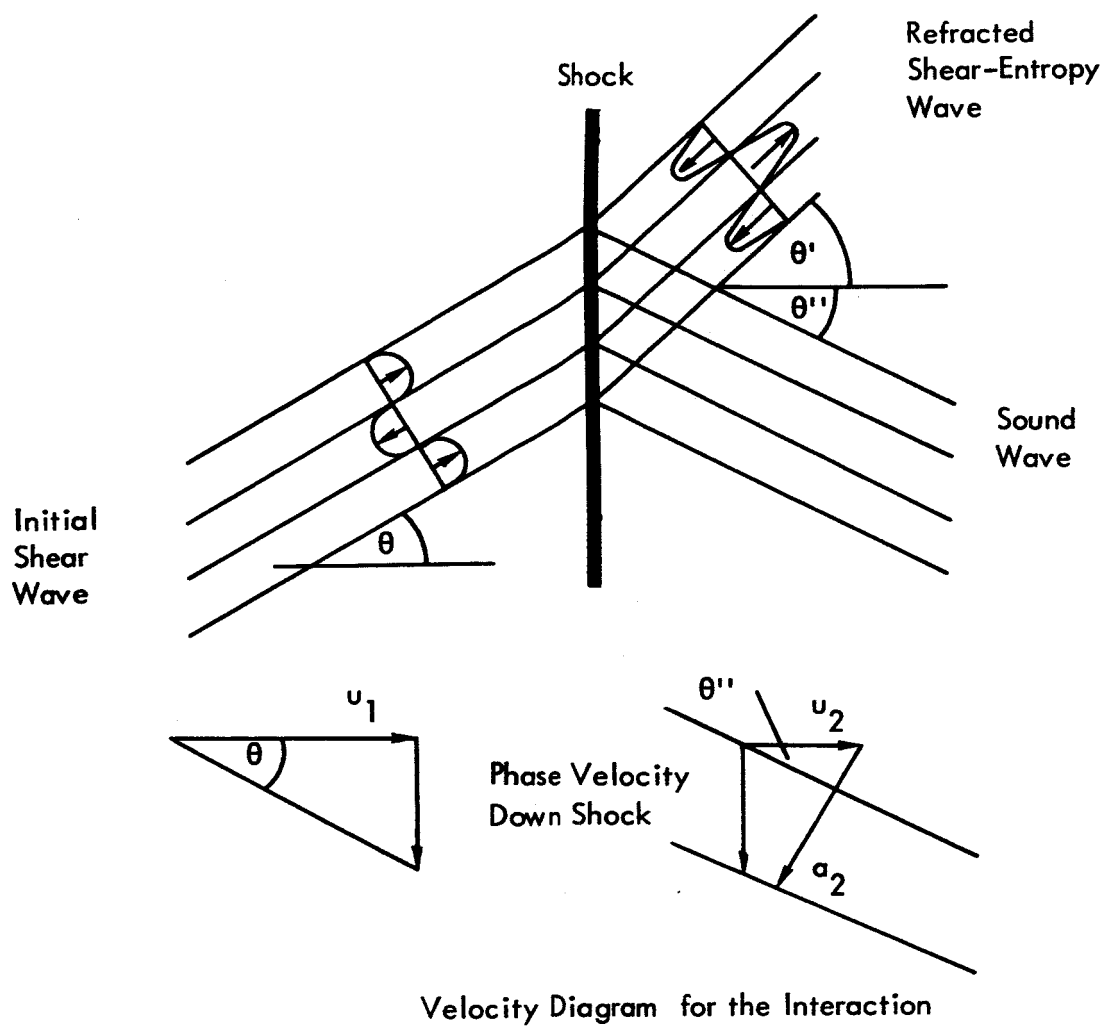


Figure 1: Interaction of a Shear Wave with a Shock.

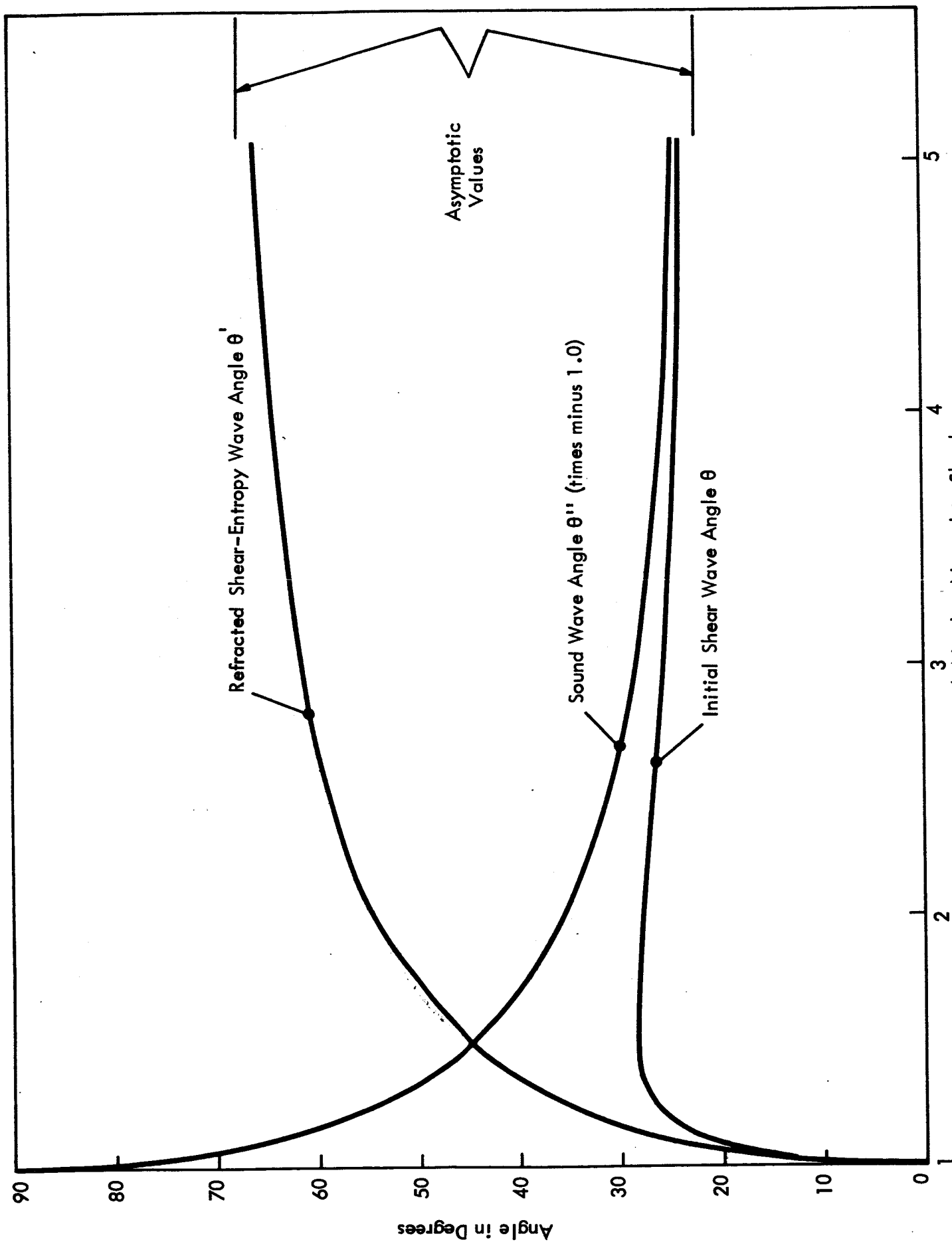


Figure 2: Wave Angles at Critical Condition, Shock-Shear Wave Interaction

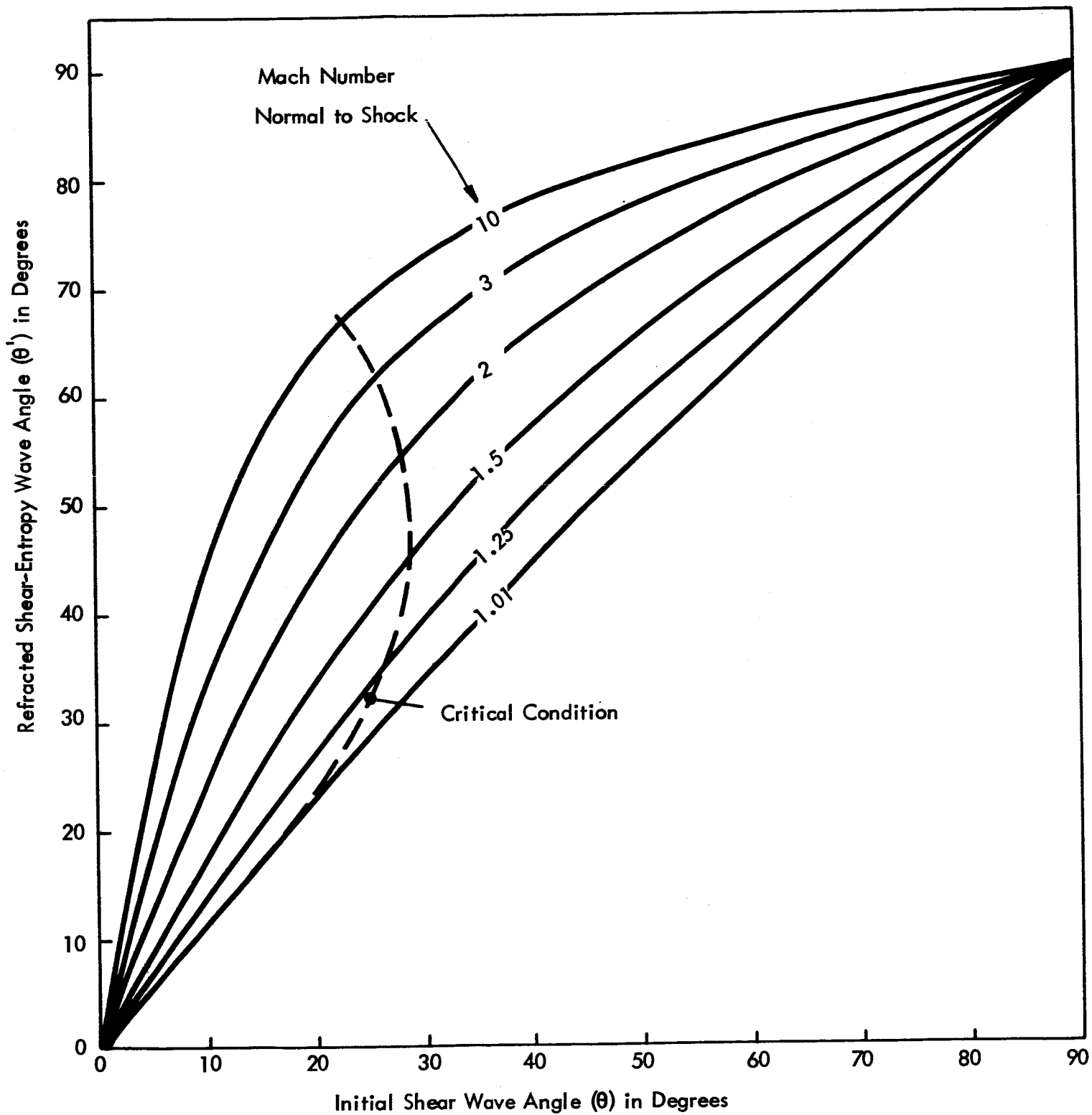


Figure 3: Refracted versus Initial Shear Wave Angle, Shock Shear Wave Interaction

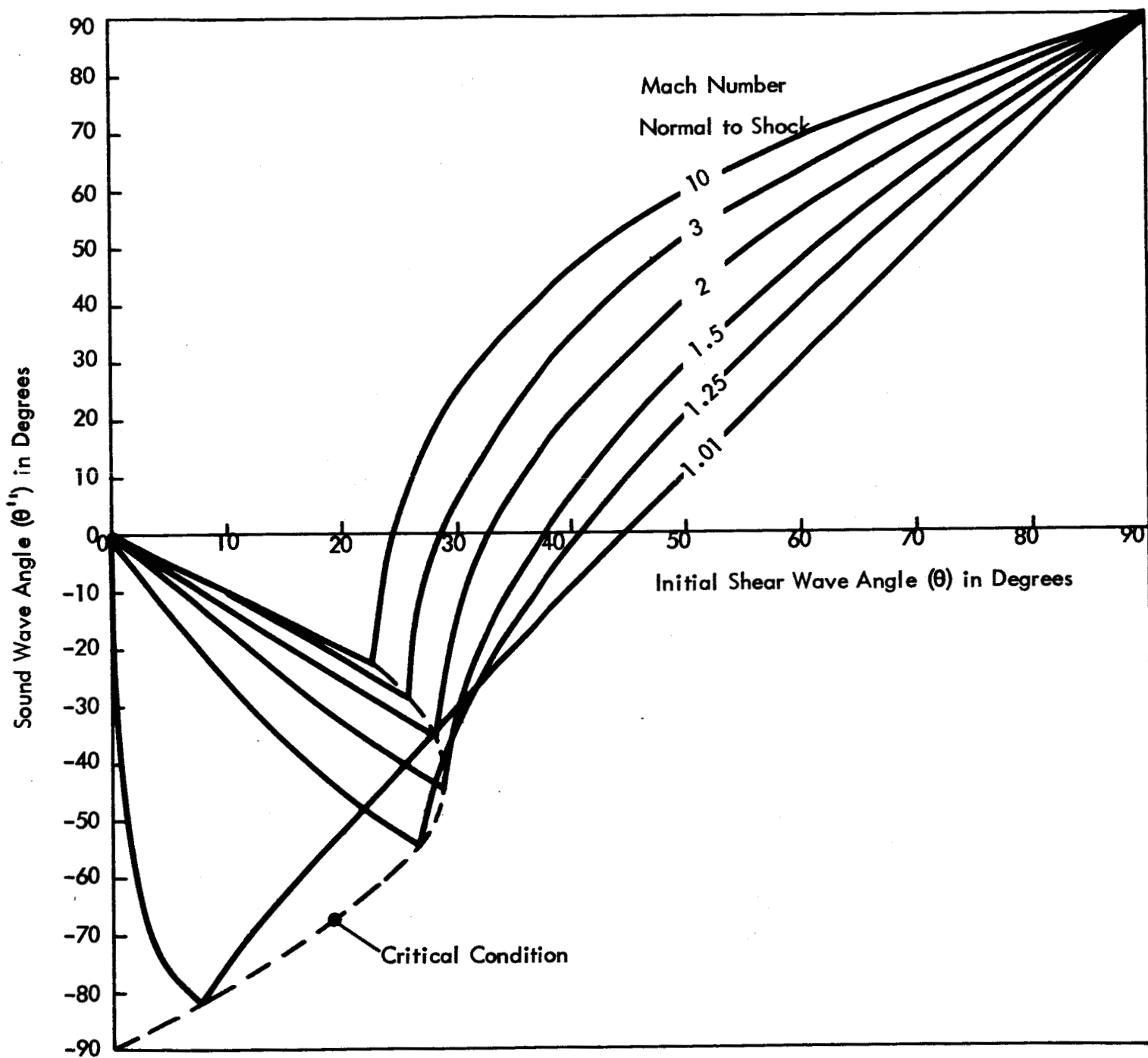


Figure 4: Sound Wave Angle versus Initial Shear Wave Angle
Shock-Shear Wave Interaction

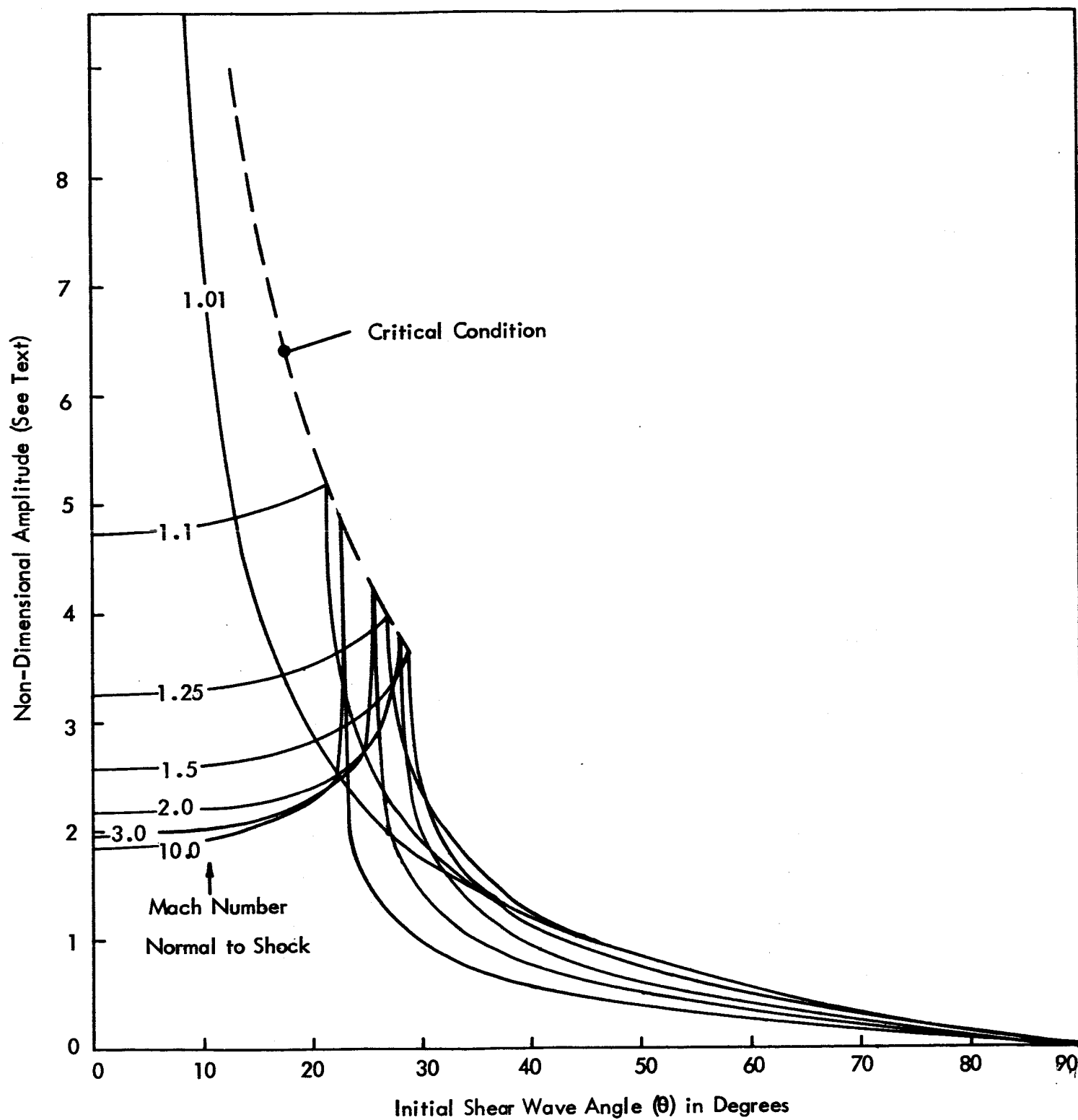


Figure 5: Amplitude of Shock Motion versus Initial Shear Wave Angle, Shock-Shear Wave Interaction

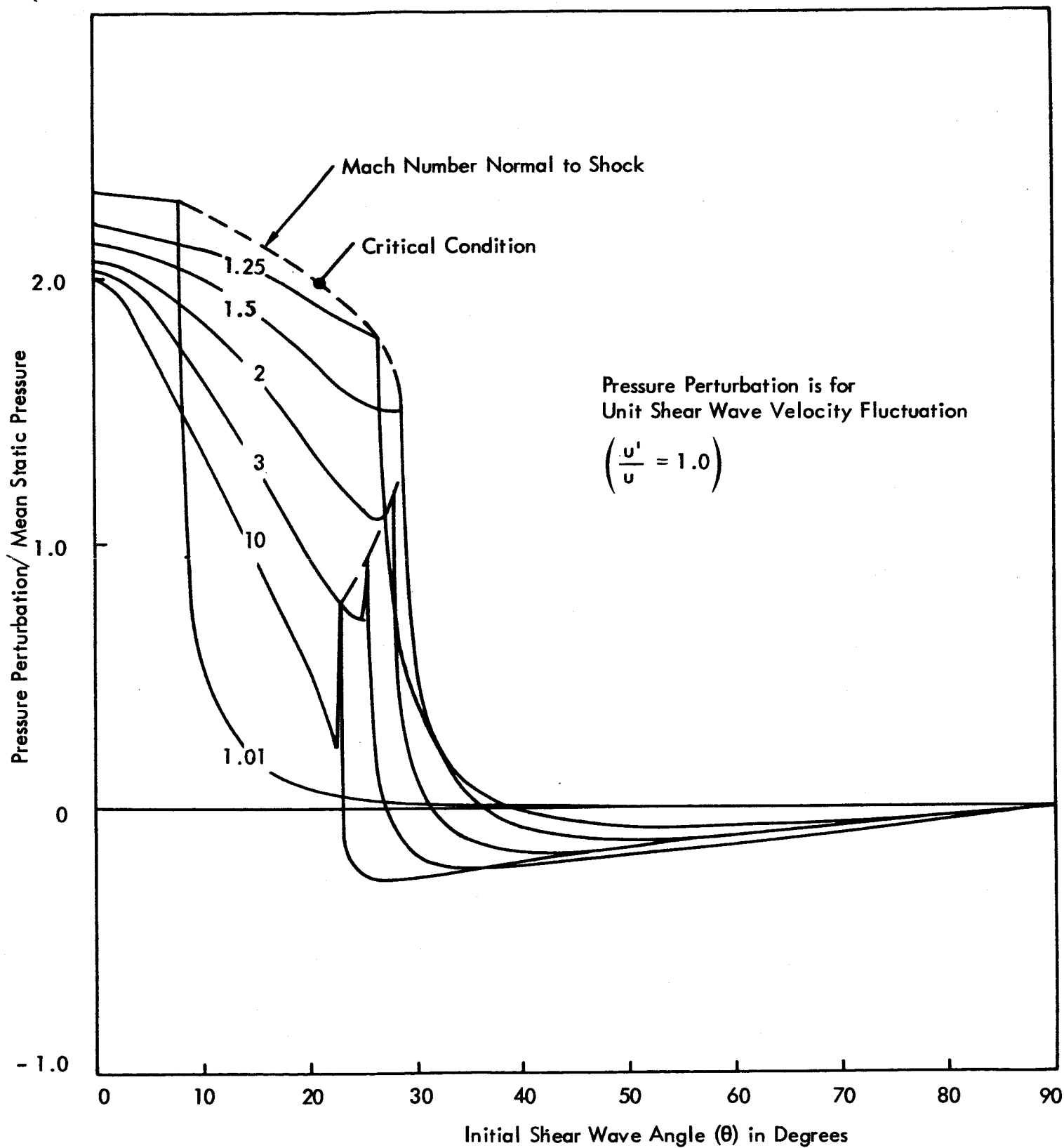


Figure 6: Pressure Fluctuation vs Shear Wave Angle, Shock-Shear Wave Interaction.

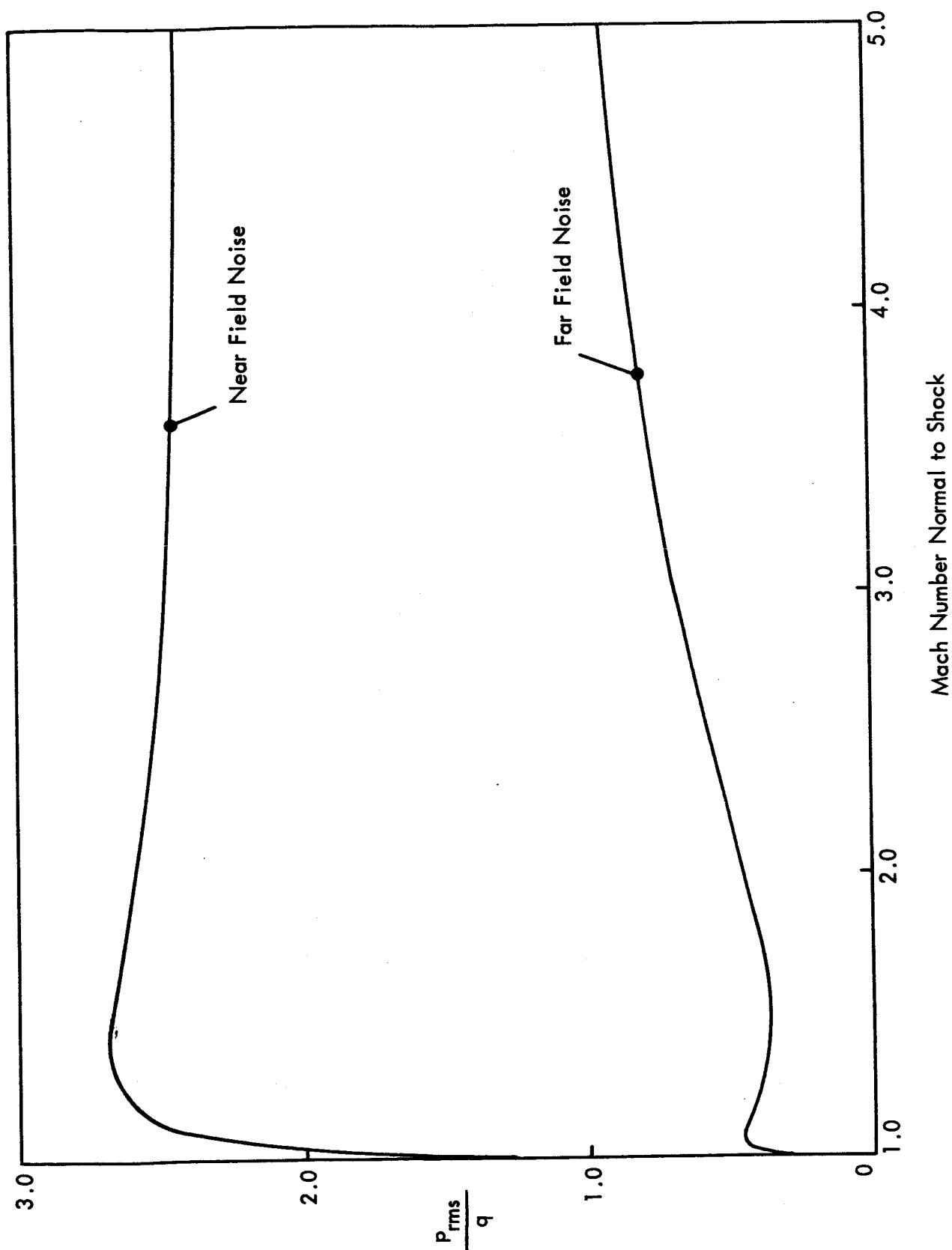


Figure 7: Near and Far Field Sound Level for Shock Interaction With Unit Isotropic Turbulence

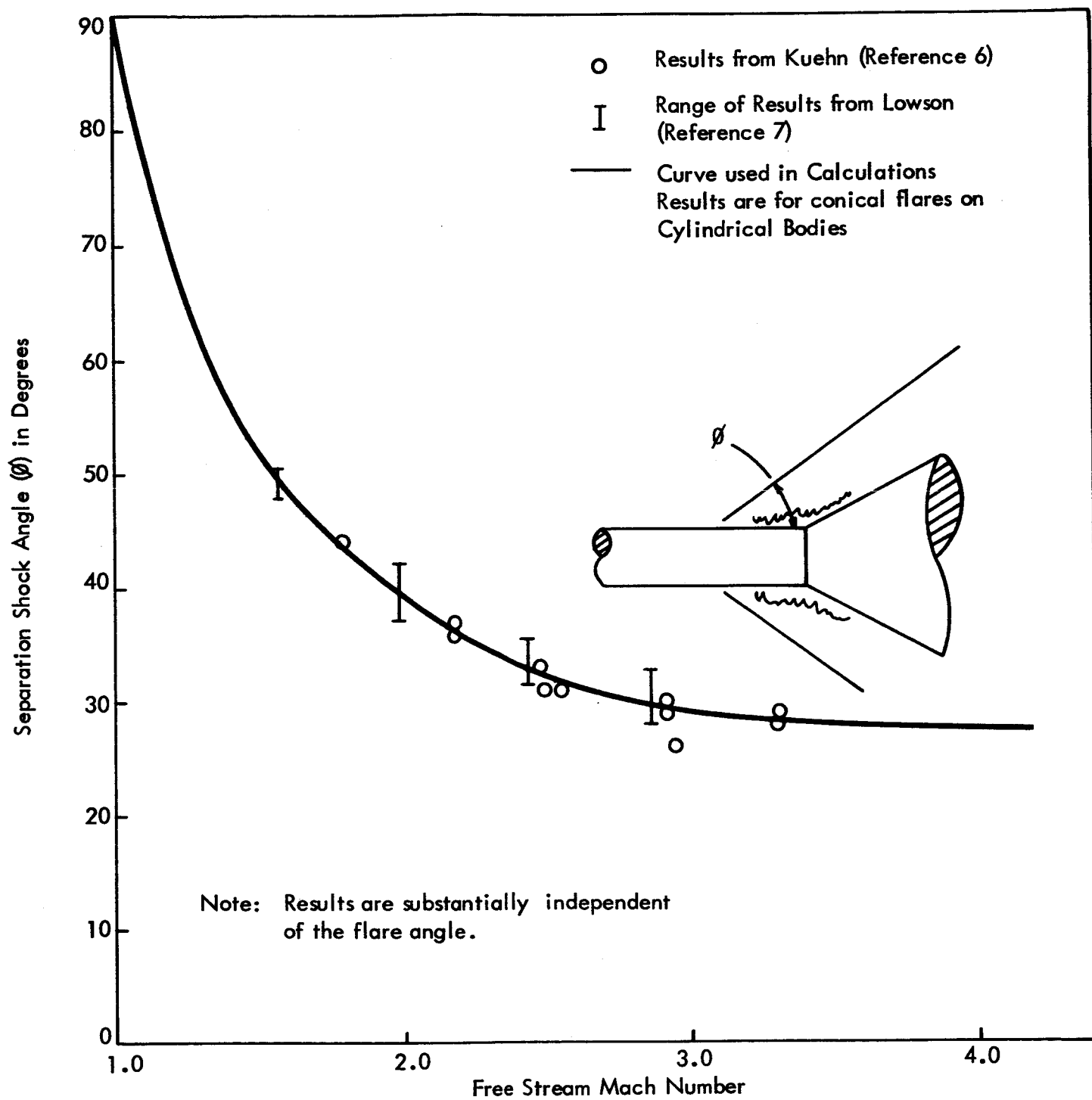


Figure 8: Separation Shock Angle versus Mach Number

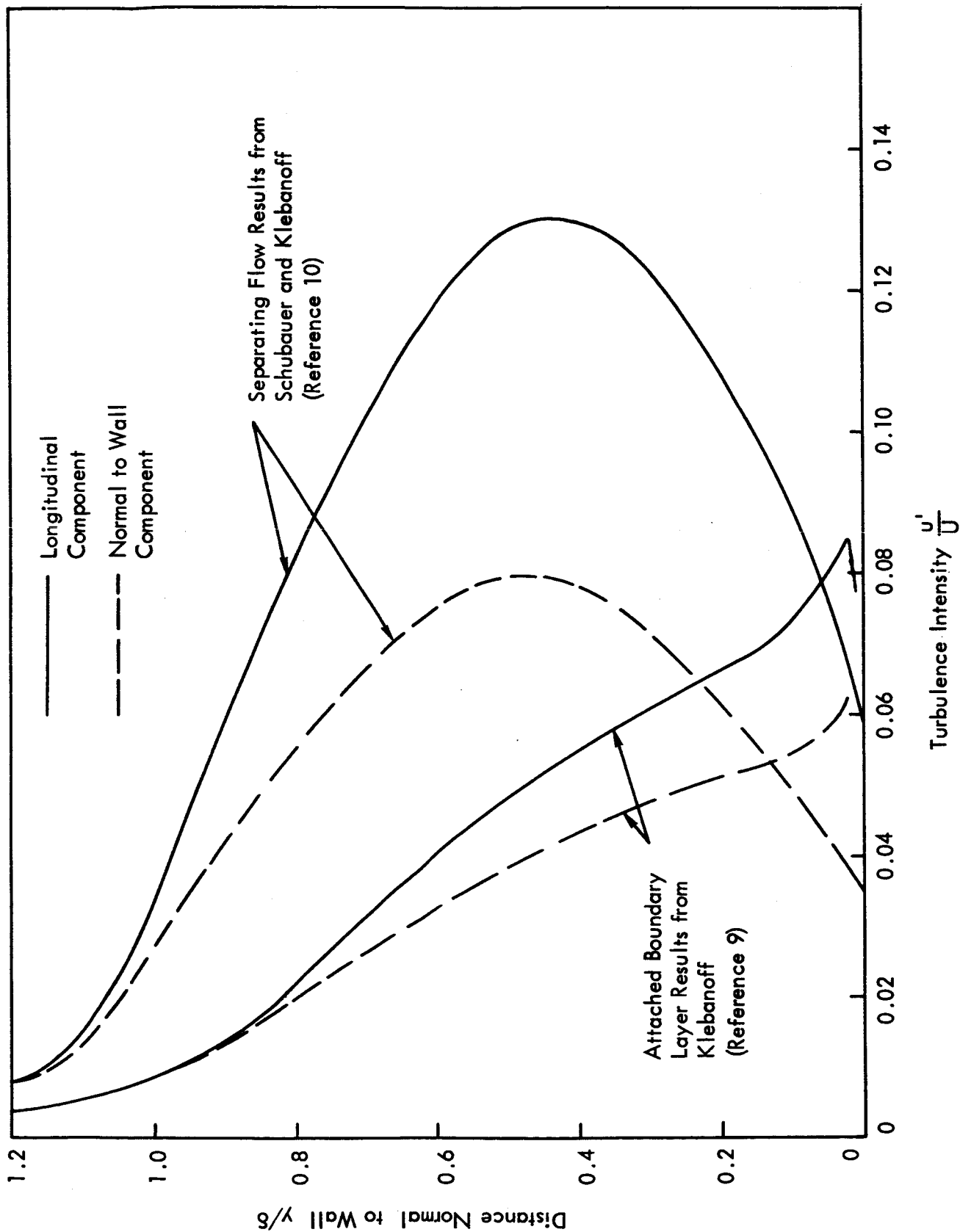


Figure 9: Turbulence Intensities in Separating and Attached Subsonic Boundary Layers.

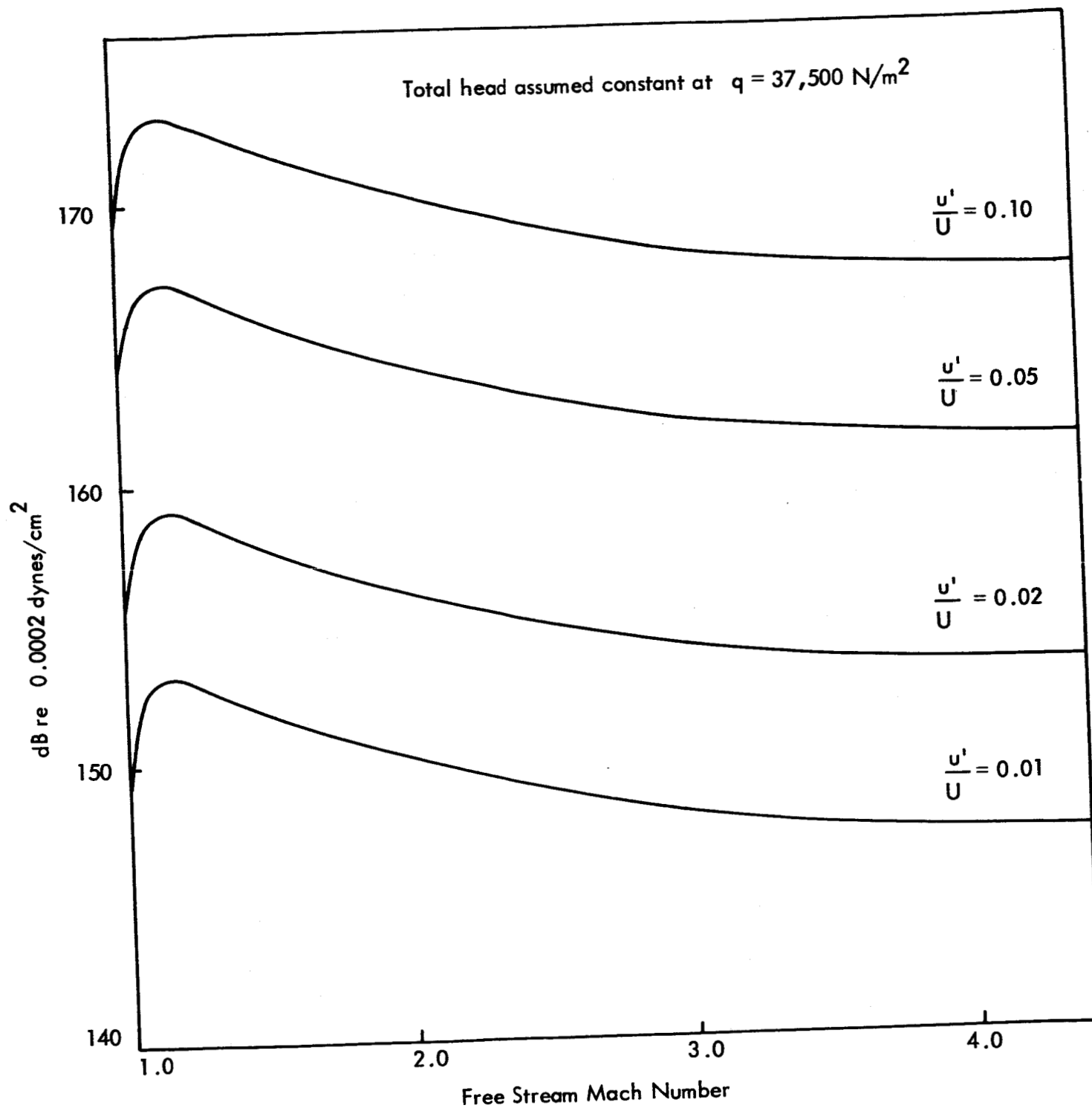


Figure 10: Calculated Near-Field Sound Levels at a Typical Separation Shock.

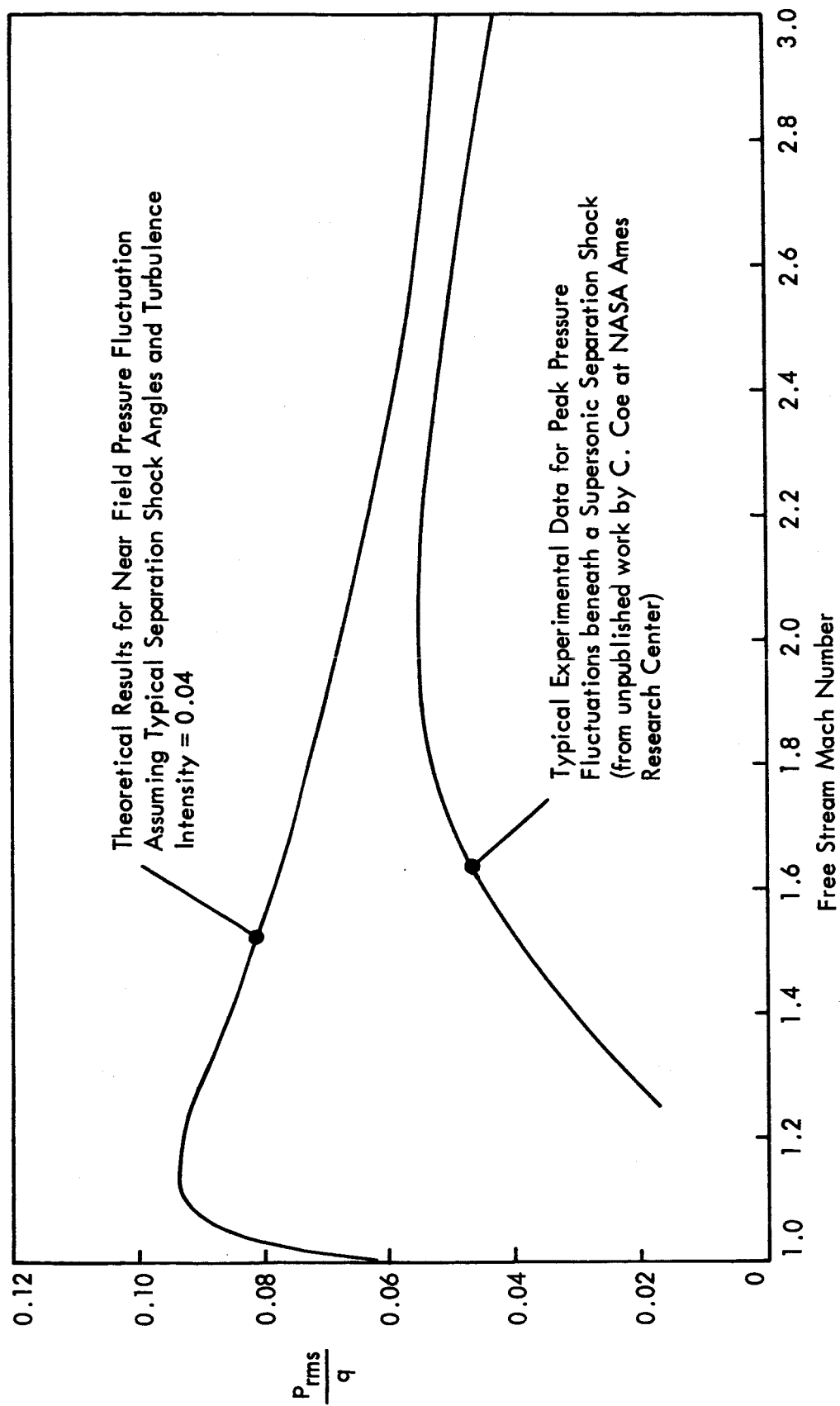


Figure 11: Comparison of Experimental Results with Present Theory at Supersonic Speeds.

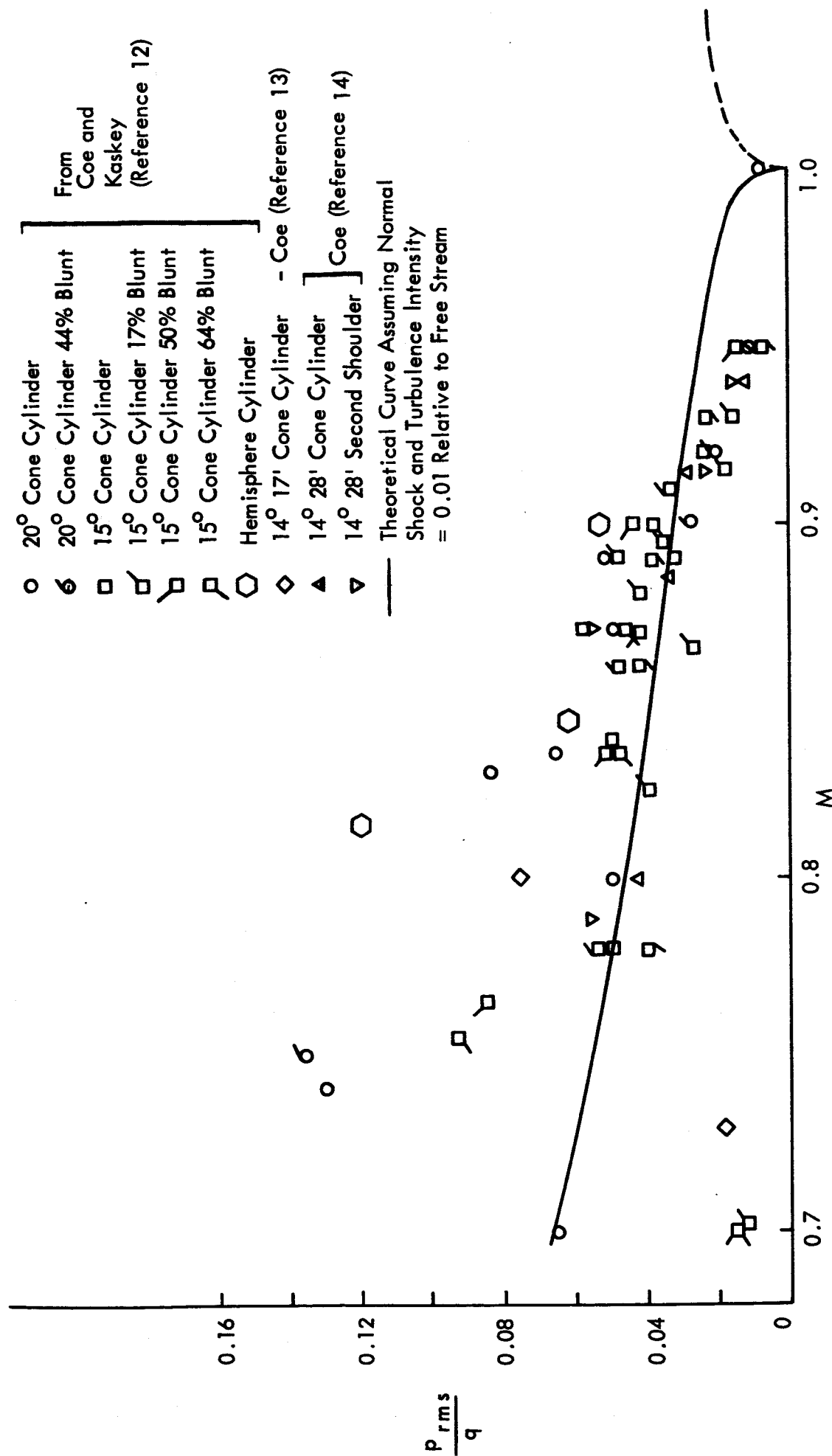


Figure 12: Fluctuating Pressure Under Transonic Oscillating Shock vs Mach Number.

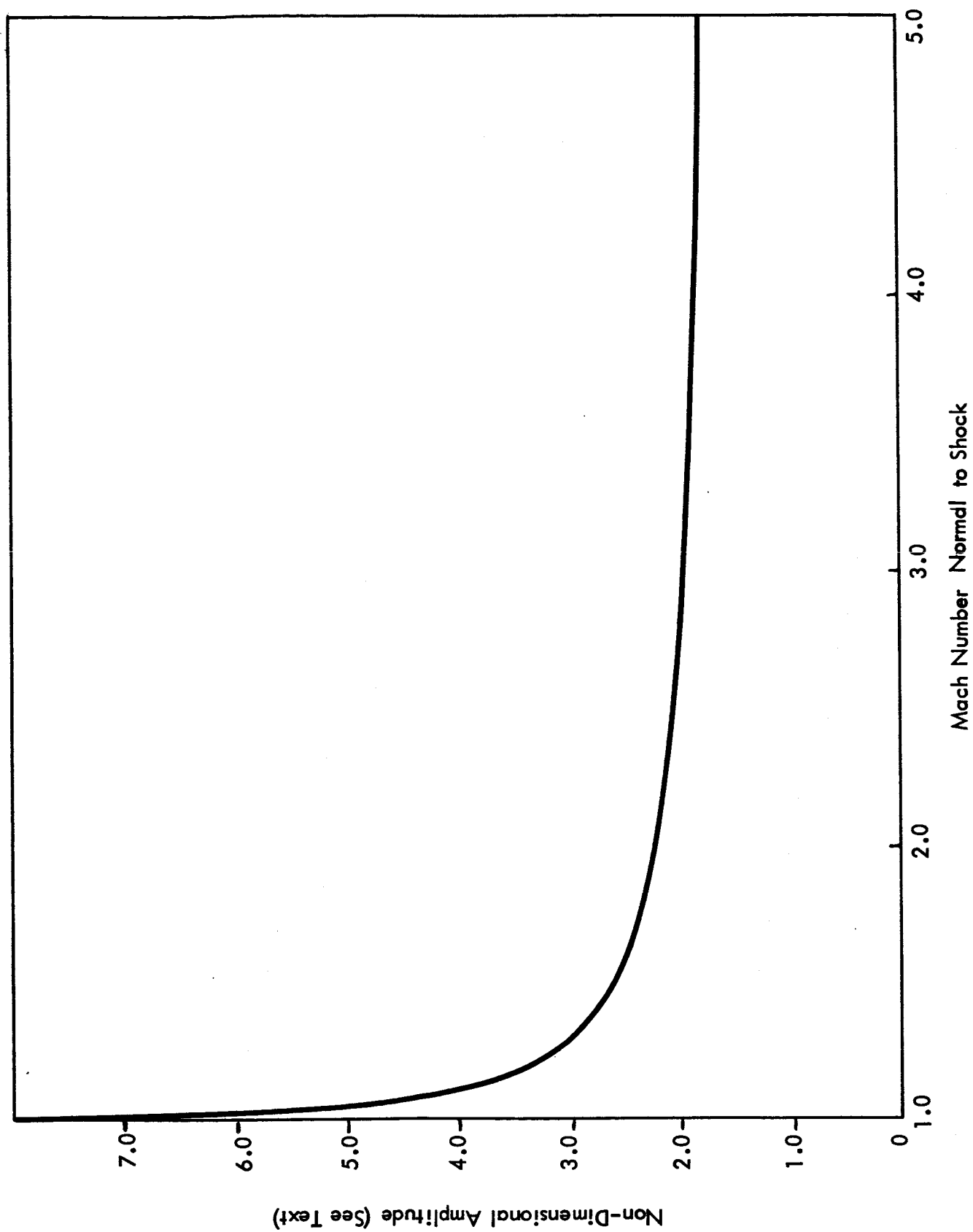


Figure 13: Amplitude versus Mach Number for Shock Turbulence Interaction

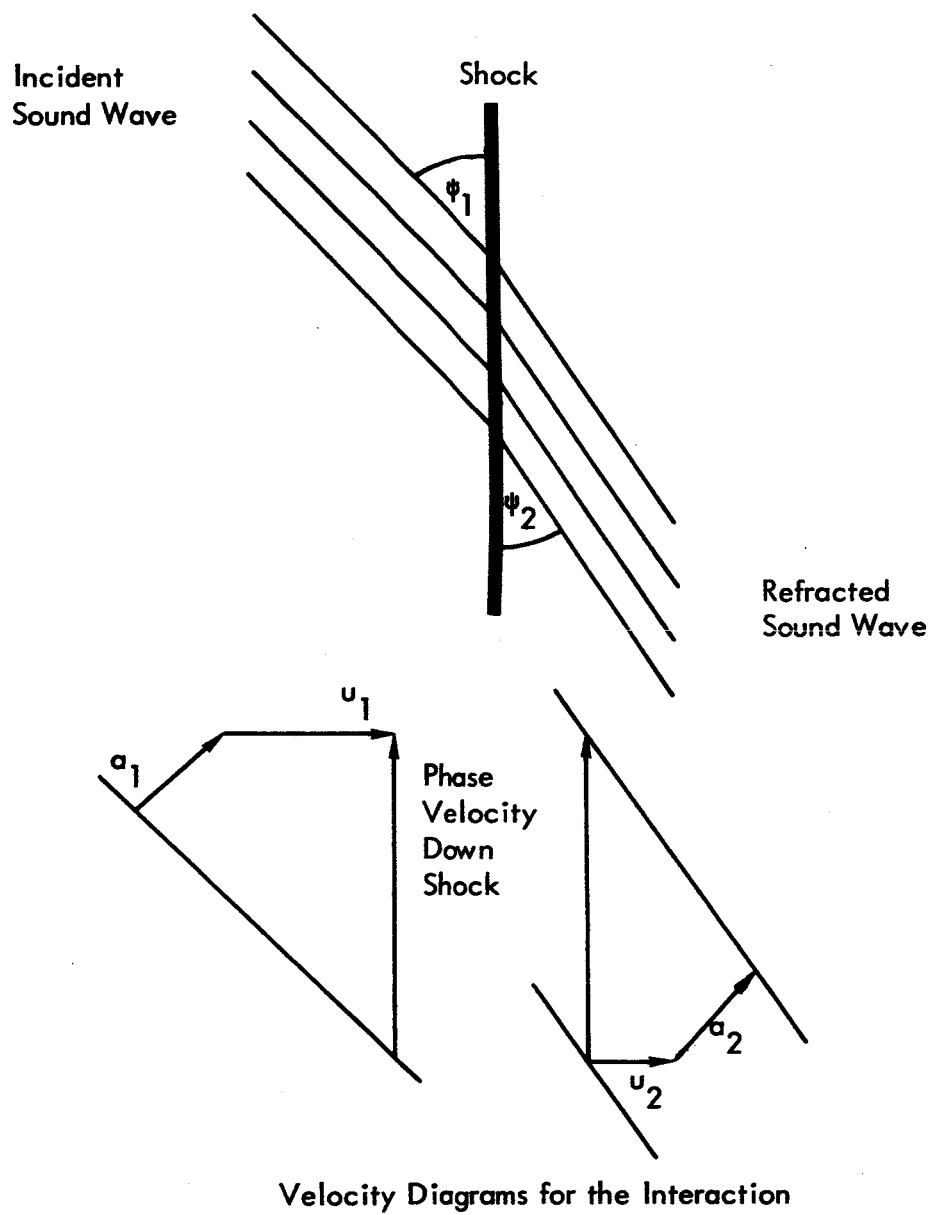


Figure 14: Interaction of a Sound Wave with a Shock.

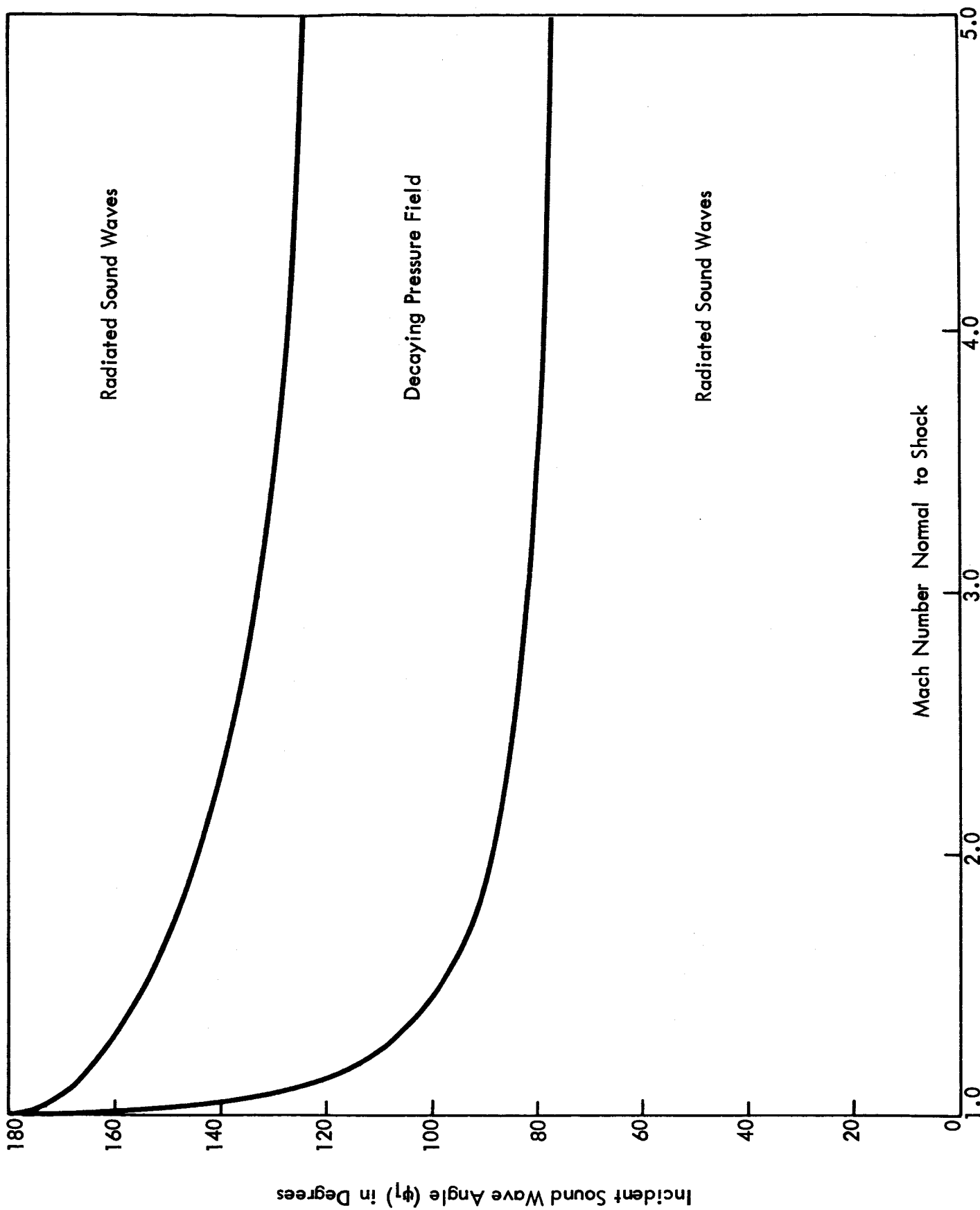


Figure 15: Critical Conditions for Shock-Sound Interactions

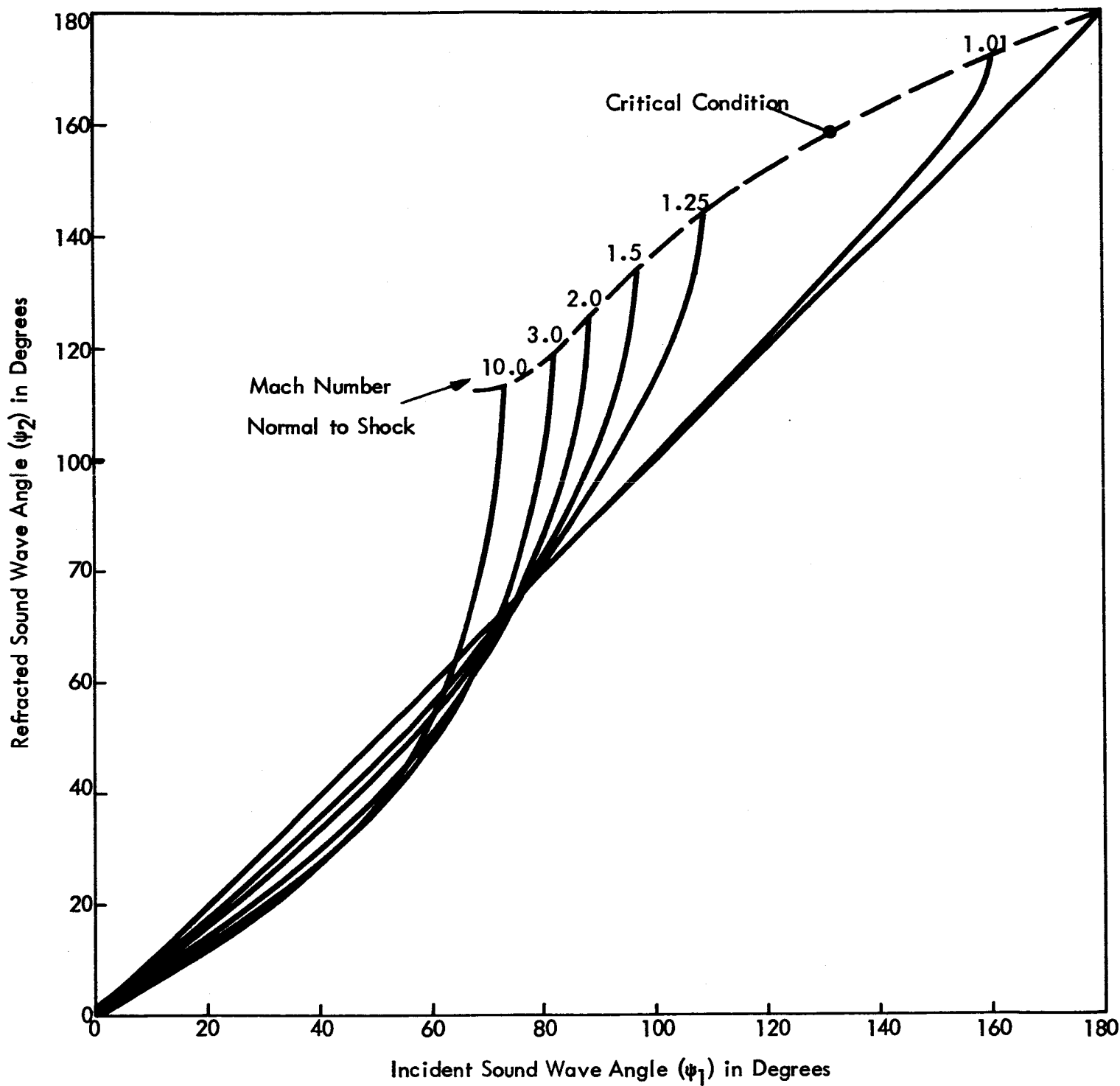


Figure 16: Incident and Refracted Wave Angles for Shock Sound Interaction

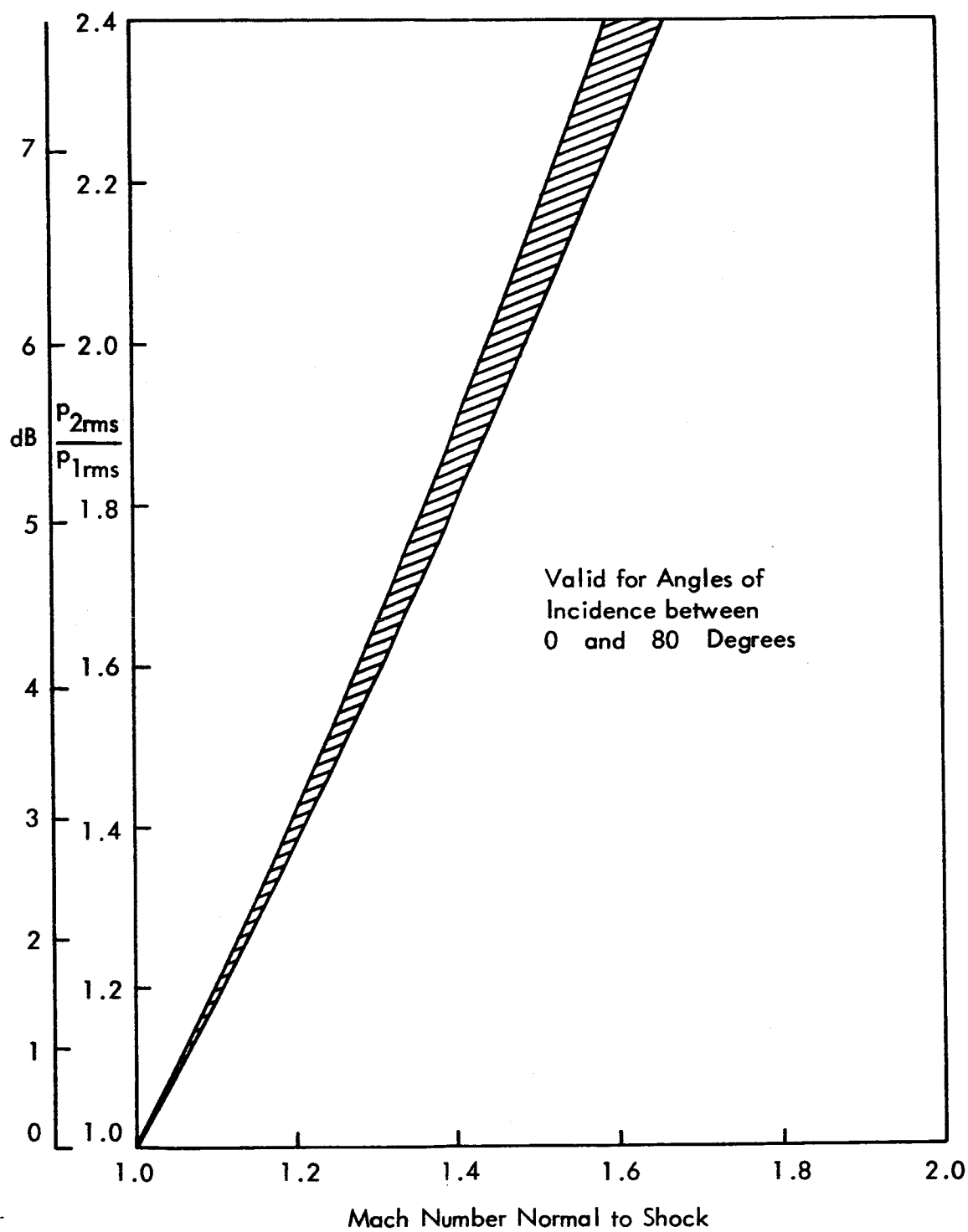


Figure 18: Range of Magnification Factor for Shock Sound Interaction.

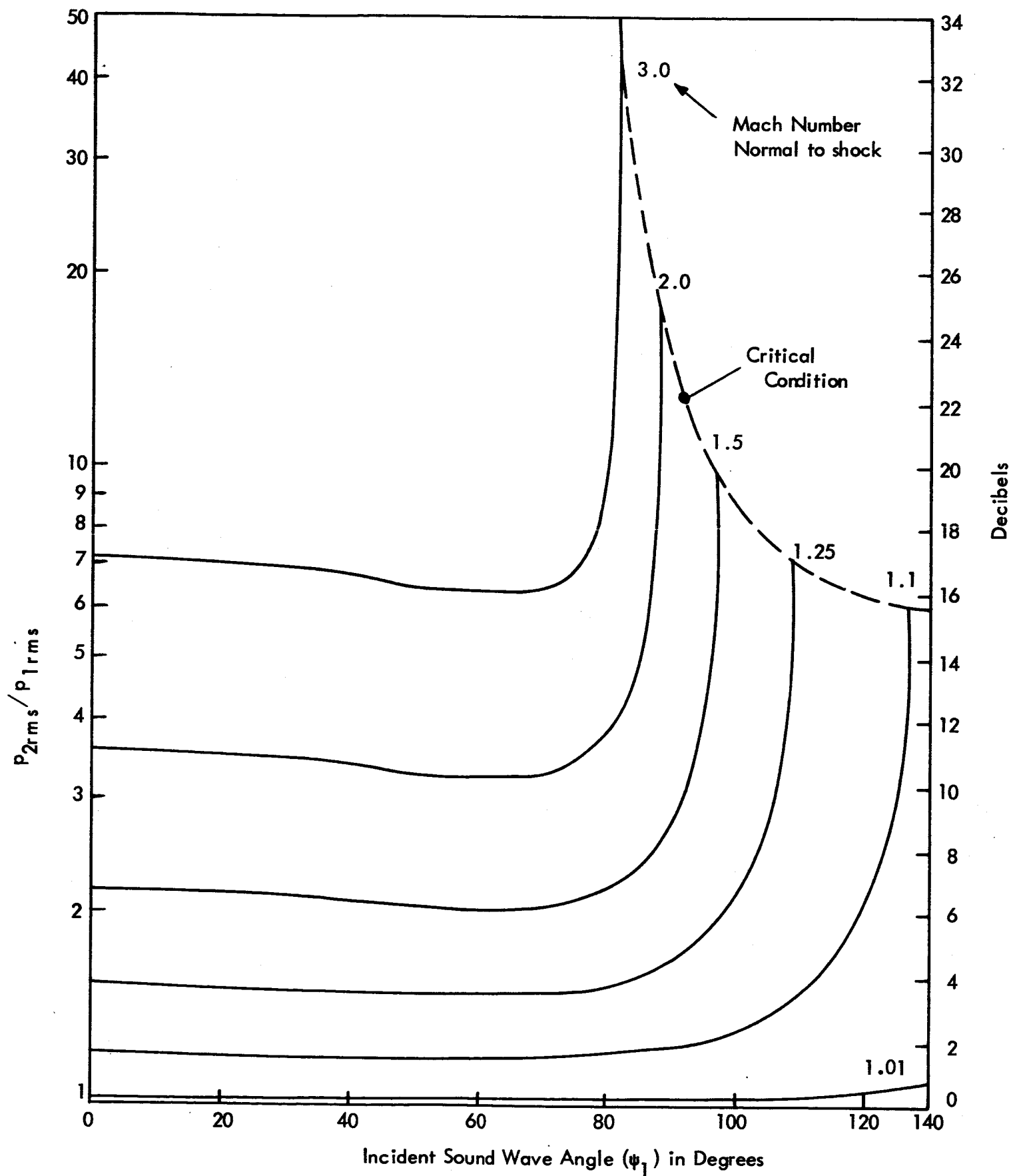


Figure 17: Pressure Magnification Factor vs Incident Sound Wave Angle, Shock-Sound Interaction.